

# E-Spun Composite Fibers of Collagen and Dragline Silk Protein: Fiber Mechanics, Biocompatibility, and Application in Stem Cell Differentiation

Bofan Zhu,<sup>†</sup> Wen Li,<sup>†</sup> Randolph V. Lewis,<sup>§</sup> Carlo U. Segre,<sup>‡</sup> and Rong Wang<sup>\*,†</sup>

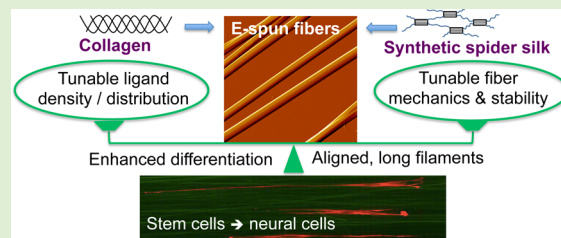
<sup>†</sup>Department of Biological and Chemical Sciences, <sup>‡</sup>Department of Physics, Illinois Institute of Technology, Chicago, Illinois 60616, United States

<sup>§</sup>Department of Biology, Utah State University, Logan, Utah 84322, United States

## S Supporting Information

**ABSTRACT:** Biocomposite matrices with high mechanical strength, high stability, and the ability to direct matrix-specific stem cell differentiation are essential for the reconstruction of lesioned tissues in tissue engineering and cell therapeutics. Toward this end, we used the electrospinning technique to fabricate well-aligned composite fibers from collagen and spider dragline silk protein, obtained from the milk of transgenic goats, mimicking the native extracellular matrix (ECM) on a similar scale. Collagen and the dragline silk proteins were found to mix homogeneously at all ratios in the electrospun (E-spun) fibers.

As a result, the ultimate tensile strength and elasticity of the fibers increased monotonically with silk percentage, whereas the stretchability was slightly reduced. Strikingly, we found that the incorporation of silk proteins to collagen dramatically increased the matrix stability against excessive fiber swelling and shape deformation in cell culture medium. When human decidua parietalis placental stem cells (hdpPSCs) were seeded on the collagen–silk matrices, the matrices were found to support cell proliferation at a similar rate as that of the pure collagen matrix, but they provided cell adhesion with reduced strengths and induced cell polarization at varied levels. Matrices containing 15 and 30 wt % silk in collagen (CS15, CS30) were found to induce a level of neural differentiation comparable to that of pure collagen. In particular, CS15 matrix induced the highest extent of cell polarization and promoted the development of extended 1D neural filaments strictly in-line with the aligned fibers. Taking the increased mechanical strength and fiber stability into consideration, CS15 and CS30 E-spun fibers offer better alternatives to pure collagen fibers as scaffolds that can be potentially utilized in neural tissue repair and the development of future nanobiodevices.



## INTRODUCTION

Collagen represents one of the most abundant structural proteins that form the extracellular matrix (ECM) of vertebrates. As a biopolymer, collagen has been frequently used as scaffolds for tissue engineering.<sup>1–3</sup> Collagen type I is the major component of tendon, skin, and artery walls. It provides the mechanical stability for tissues and serves as a functional environment for cells.<sup>4,5</sup> As an ECM protein, collagen type I supports the attachment and growth of cells, particularly many neuronal cell types.<sup>6,7</sup> Mediated by the collagen–β-1 integrin interaction, collagen type I is known to promote the neural differentiation of stem cells in both neural differentiation medium<sup>7,8</sup> and spontaneous differentiation medium.<sup>9,10</sup> *In vitro* studies have shown that exogenous collagen type I forms a network of interconnected fibers upon gelation, and the self-assembly process results in random dimension, morphology, and orientation of collagen fibers. Native fibrillar collagen type I is typically aligned in parallel arrays in connective tissues, either locally or extensively.<sup>11–13</sup> Such aligned matrices can provide guidance for neural cell migration and directional axonal regeneration, which is a key engineering target for neural repair.<sup>14</sup> It is highly desirable to

construct aligned collagen fibers to mimic the native tissue environment for *in vitro* studies.

Electrospinning has been applied to the fabrication of polymer and protein fibers with architectures similar to those naturally occurring in the extracellular environment.<sup>15</sup> It is remarkably efficient, inexpensive, and allows easy incorporation of additional components to make composite fibers.<sup>16</sup> In this work, by using a home-built electrospinning system, we were able to fabricate unidirectionally aligned collagen fibers with controllable diameters, uniform morphology, and high surface coverage. The home-built system uses parallel metal plates to collect freestanding fibers, which can be directly used for mechanical tests or easily transferred to desired substrates for cross-linking, characterization, sterilization, and cell culture applications.

It was reported that an as-prepared collagen matrix is weak and unstable for long-term cell culture and thus is not a desirable scaffold for tissue engineering.<sup>17</sup> We had similar

Received: September 19, 2014

Revised: November 15, 2014

Published: November 18, 2014

observations in our previous work. A high extent of cross-linking *in vitro* can make collagen fibers physically stronger and more stable but was discovered to affect cell adhesion.<sup>18</sup> Spider silk is a promising biopolymer with remarkable tensile strength and superior elasticity. Among seven types of silk produced by the golden orb weaver spider *Nephila clavipes*, dragline silk is the strongest due to its main composition of major ampullate spidroins 1 and major ampullate spidroins 2 (MaSp 1 and MaSp 2).<sup>19</sup> The coexistence of an alanine-rich motif (highly organized  $\beta$ -sheet crystalline domain) and a glycine-rich motif (amorphous matrix) in dragline silk renders a unique combination of high tensile strength and extensibility.<sup>20</sup> The native dragline silk has Young's modulus and ultimate tensile strength of 22 and 1.1 GPa, respectively,<sup>21</sup> in comparison to 1.2 and 0.12 GPa for native collagen fibers.<sup>22,23</sup> However, unlike collagen, silk proteins are not ECM proteins; accordingly, they do not adequately support cell adhesion, growth, and differentiation. To create mechanically strong, stable, and biocompatible matrices, we integrated collagen with MaSp1 and MaSp2 proteins, which were extracted and purified from the milk of transgenic goats.<sup>24</sup> While silk fibroin is also a good candidate for generating collagen–silk biocomposite scaffolds to achieve improved fiber stability<sup>25</sup> and to support cell adhesion and proliferation,<sup>26</sup> the composite fibers are mechanically weak, with a tensile strength of less than 2 MPa.<sup>26</sup> The tensile strength of the collagen–dragline silk composite fibers in this study is 10 to 100 times higher. Collagen and dragline silk proteins were mixed at various ratios, electro-spun (E-spun), and lightly cross-linked to form composite fibers. In addition to biocompatibility studies, the unidirectional aligned collagen–dragline silk composite fibers were applied as a matrix to examining the stem cell differentiation.

We used human decidua parietalis placental stem cell (hdpPSC) as a model system in this study. hdpPSCs are multipotent adult stem cells derived from the maternal side of human placenta. They are robust, easily derived, and preferable for *in vitro* studies and clinical therapies.<sup>27,28</sup> The unidirectionally aligned scaffolds of collagen-dominant composites were found to provide unique structural, mechanical, and biochemical cues to direct stem cell polarization and neural differentiation, to facilitate the development of long neural filaments, and to orient the neural filaments along the fibers. They offer potential solutions for transplantation in cellular replacement therapies for neurodegenerative disorders such as Alzheimer's and Parkinson's diseases,<sup>9</sup> and they open a new avenue for neural tissue engineering and fabrication of future nanobiodevices.<sup>14,29</sup>

## EXPERIMENTAL SECTION

**Materials.** Collagen type I from calf skin was purchased from MP Biomedicals (Solon, OH). Major ampullate spidroin proteins 1 and 2 (MaSp 1 and MaSp 2) of dragline spider silk were extracted from the milk of transgenic goats and analyzed by SDS-PAGE and western blot, with purities higher than 95%.<sup>30</sup>

The silk proteins were mixed at a MaSp1/MaSp2 ratio of 4:1 to obtain optimized mechanical properties.<sup>24</sup> Collagen and silk proteins were dissolved in 1,1,1,3,3-hexafluoro-2-propanol (HFIP) (Fisher Scientific, Pittsburgh, PA) separately, and the solutions of collagen and silk protein were mixed to make solutions containing silk at 0% (pure collagen), 15% (CS15), 30% (CS30), 60% (CS60), and 100% (pure silk). The total protein content was maintained at 100 mg/mL in all protein solutions.

**Home-Built Electrospinning System for Collecting Free-standing Fibers.** A home-built electrospinning system (see Figure S1) was used in this study to fabricate freestanding collagen-silk composite fibers. A 0.2 mL protein solution was placed in a 1.0 mL syringe with an 18-gauge blunt needle (Fisher Scientific, Pittsburgh, PA) to produce continuous microfibers. A voltage of 15–25 kV was applied to the metal needle by a high-voltage power supply (Glassman High Voltage, High Bridge, NJ). A syringe pump (Harvard Bioscience Inc., Holliston, MA) was used to deliver the protein solution at a constant flow rate. Two parallel metal plates were grounded and placed 6–10 mm apart and 10–20 cm below the needle, serving as the collector of protein fibers. Due to the electrostatic interactions, the E-spun fibers were aligned and stretched across the two plates.<sup>31,32</sup> Fiber density can be controlled by varying the collection time. A collection time of 30 s was chosen in this study to achieve a relatively low fiber density, allowing a cell to adhere to an individual fiber for effective cell polarization, differentiation, and the development of long filament unidirectionally. Electrospinning parameters, such as electric potential, air gap distance, delivery rate, and collector gap, were optimized to achieve well-aligned, uniform fibers with high surface coverage. The parameters used in this study are listed in Table 1. The freestanding

**Table 1. Electrospinning Parameters for the Preparation of Collagen–Silk Composite Fibers**

protein composition	collagen and silk
solution concentration	100 mg/mL
electric potential	25 kV
air gap distance	150 mm
delivery rate	5 mL/h
gap of collector	8 mm/10 mm
collection time	30 s
needle gauge	18 G blunt

fibers were collected directly on pre-cut frames (made from aluminum foil) for mechanical tests or transferred onto pre-cut glass slides for microscopic characterization and cell culture. Prior to any test, the fibers were cross-linked by exposing to glutaraldehyde (20% v/v, Fisher Scientific, Pittsburgh, PA) vapor for 12 h at room temperature. Fibers for cell culture were sterilized by 70% (v/v) ethanol and an overnight UV treatment.

**Atomic Force Microscopic (AFM) Imaging.** Imaging was carried out by using a multimode Nanoscope IIIa AFM (Veeco Metrology, Santa Barbara, CA) equipped with a J-scanner. Images of various E-spun fibers were collected in fluid-tapping mode in PBS buffer using Si<sub>3</sub>N<sub>4</sub> tips (K-Tek Nanotechnology, Wilsonville, OR) at a frequency of 8–10 kHz. From obtained images, the width and height of the five types of fibers (collagen, CS15, CS30, CS60, and silk) were analyzed using NanoScope Analysis software. The cross-sectional area of these fibers was evaluated on the basis of cross-sectional analysis (Figure S2). For statistical analysis, 20–30 fibers were analyzed on each sample, and more than 20 samples were examined for each fiber type.

**Mechanical Testing.** Mechanical properties of E-spun fibers were examined by stress–strain analysis using a MTS Synergie 100 system (Test Resources Inc., Shakopee, MN). Fibers were collected on a pre-cut, U-shaped frame of aluminum foil that covered the grounded, parallel metal plates serving as the fiber collectors. The two long sides (4 cm long) of the U-shaped frame were 10 mm apart. An array of aligned fibers were collected on the frame across the gap and were glued at the edge of the frame. After cross-linking, disordered and nonuniform fibers, typically away from the center of the matrix, were carefully removed, leaving 2 cm wide, uniformly distributed, unidirectionally aligned fiber arrays at the center of the frame. Optical images (20 $\times$ ) were collected along the long side of the frame at both edges to count the number of fibers per unit width of the matrix. After the frame was loaded on the test machine and the narrow side of the frame was cut, fibers spanning across the 10 mm gap were stretched along the fiber direction at a rate of 1 mm/min. Load vs stretching displacement curves were collected at a data acquisition rate of 120

Hz. From each curve of fiber type  $i$ , the maximum loading force ( $F_{i,\max}$ ) and the stretching distance at the fracture point ( $\Delta x_{i,\max}$ ) were recorded, and the ultimate tensile strength ( $\sigma_{i,\max}$ ) and ultimate strain ( $\epsilon_{i,\max}$ ) were then calculated by the equations below

$$\sigma_{i,\max} = \frac{F_{i,\max}}{S_i \cdot n_i \cdot l} \quad (1)$$

and

$$\epsilon_{i,\max} = \frac{\Delta x_{i,\max}}{X} \quad (2)$$

where  $S_i$  is the average cross-sectional area of fiber type  $i$  predetermined by AFM measurements (Figure S2),  $n_i$  is the number of fibers per unit width of the matrix measured from optical images,  $l$  (2 cm) is the width of the matrix (perpendicular to the fiber alignment) subjected to the mechanical test, and  $X$  (1 cm) is the length of the tested fibers. The denominator of eq 1,  $S_i \cdot n_i \cdot l$ , is equivalent to the cross-sectional area of the tested fiber matrix. Young's modulus,  $E$ , as the ratio of tensile strength and tensile strain in the elastic deformation range,<sup>33</sup> can be calculated from the slope ( $k_i$ ) of the linear portion of a load vs displacement curve using the equation below

$$E_i = \frac{k_i \cdot X}{S_i \cdot n_i \cdot l} \quad (3)$$

More than 25 measurements were conducted under the same conditions for each fiber type for statistical analysis.

**Infrared Spectroscopy.** Infrared spectra of E-spun fibers were collected using a Thermo Nicolet Nexus 470 FTIR Spectrometer (Thermo Electron Co., Madison, WI). E-spun fibers were similarly collected on pre-cut aluminum frames under the same E-spin conditions mentioned above. After overnight drying in a vacuum desiccator, the frame with fibers was loaded onto the sample holder. Fibers at the gap region were exposed to the IR beam and were scanned directly in the range of 400–4000  $\text{cm}^{-1}$  with a nominal resolution of 4  $\text{cm}^{-1}$ .

**Cell Culture of hdpSCs on Various Matrices.** Undifferentiated hdpSCs were kindly provided by Dr. Zuzana Strakova (UIC, Chicago, IL).<sup>34</sup> The cells were maintained in a self-renewal state in phenol red-free RPMI-1640 medium (Invitrogen, Carlsbad, CA) supplemented with 0.1 mM sodium pyruvate, 100 U/mL penicillin-streptomycin (Sigma-Aldrich, St. Louis, MO), and 10% charcoal-stripped fetal bovine serum (S-FBS).

Prior to cell culture, the sterilized E-spun matrices were placed in a 24-well culture plate, and a sterilized glass slide without fibers was used as a control. Undifferentiated hdpPSC cells at passages 3–5 were then trypsinized and seeded at a density of 2000 cells/ $\text{cm}^2$  on various matrices in a nonselective, spontaneous differentiation medium of Dulbecco's modified Eagle's medium (DMEM) supplemented with 10% fetal bovine serum and 1% nonessential amino acids.<sup>9</sup> The medium was changed every other day.

**Optical Imaging.** Fiber alignment and surface coverage were analyzed by a Nikon TE 2000-U microscope. Collagen's autofluorescence allows the examination of collagen expression level. Collagen expression was also studied by immunostaining with rabbit anti-collagen type I (Abcam, Cambridge, MA, 1:200 dilution).

The expressions of nestin,  $\beta$ -III tubulin, and NeuN in cells on various matrices were examined at days 1, 3, and 5 of cell differentiation.  $\beta$ -1 integrin expression was examined at 6 and 12 h post-plating to study cell adhesion. In each experiment, the cells were fixed by 4% paraformaldehyde for 10 min at room temperature and permeabilized with 0.1% Triton X-100 in PBS for 10 min. The cells were then blocked with 1% BSA in PBST (PBS with 0.5% Tween-20) for 1 h before overnight incubation with primary antibodies at 4 °C. Primary antibodies used in this study include rabbit anti-integrin  $\beta$ -1 (Santa Cruz Biotechnology, Dallas, TX, 1:100 dilution), mouse anti-nestin (Millipore, Billerica, MA, 1:200 dilution), rabbit anti- $\beta$ -III tubulin (Abcam, Cambridge, MA, 1:200 dilution), and mouse anti-NeuN (Millipore, Temecula, CA, 1:100 dilution). Secondary antibod-

ies were purchased from Invitrogen (Carlsbad, CA) and used at a dilution of 1:200. The nuclei were stained with DAPI at a 1:1000 dilution for 10 min at room temperature. The exposure time and gain value were kept constant for each marker across all samples, and a negative control was performed by excluding the primary antibody during the staining protocol for each set of experiments.

The immunofluorescent images were quantitatively analyzed by ImageJ software. Constant image size, magnification, and imaging parameters were used for all measurements, and the background was subtracted for fluorescence intensity measurements. The positive cells were defined as cells with fluorescence intensity three times or more above the background level.

**Cell Proliferation and Polarization Studies.** The proliferation of hdpPSCs on E-spun fibers was examined by collecting fluorescent images of cells cultured on each matrix type at days 1, 3, 5, and 7. Cell number per unit area was counted on the basis of DAPI staining on more than 20 images (4 $\times$ ) for each matrix type.

The change of hdpPSC morphology was monitored during cell differentiation between 0 h and 5 days. Cell length and cell area at each time point were measured from 20 $\times$  phase-contrast images using ImageJ software. The effective cell width was determined using the ratio of cell area to cell length. Cell polarity was then characterized by the cell length-to-width ratio

$$\text{cell polarity} = \frac{\text{cell length}}{\text{effective cell width}} = \frac{\text{cell length}^2}{\text{cell area}} \quad (4)$$

**Trypsin De-adhesion Assay.** hdpPSCs after 6 and 12 h culture in nonselective differentiation medium were washed with PBS and placed under the optical microscope. After 100  $\mu\text{L}$  of 0.05% trypsin-EDTA (Invitrogen, Carlsbad, CA) was added to the cells, 20 $\times$  images were taken *in situ* every 15 s to monitor the reduction in cell-substrate contact area until no change was detectable. The change in the contact area with time was plotted, and the earliest saturation time was derived. The normalized area,  $A_{\text{normalized}}$ , is defined as the ratio of the change in area from initial time point to the given time ( $A_{\text{init}} - A_t$ ) and the total change in area ( $A_{\text{init}} - A_{\text{final}}$ ). In the dynamic de-adhesion process,  $A_{\text{normalized}}$  varies from 0 to 1, and the  $A_{\text{normalized}}$  vs time curve was then fit to the Boltzmann sigmoid equation<sup>35,36</sup>

$$A_{\text{normalized}} = 1 - \frac{1}{1 + e^{(t-t_{0.5})/\tau}} \quad (5)$$

where  $t$  is a given time point and  $t_{0.5}$  and  $\tau$  are the time constants.  $t_{0.5}$  represents the time point when the area change is 50% of the total area reduction, which is used in this study to quantify the strength of cell adhesion.

## RESULTS

**Characterization of Physical Properties of Collagen–Silk Composite Fibers.** Collagen can be monitored by its strong autofluorescence. Figure 1 shows the bright field and

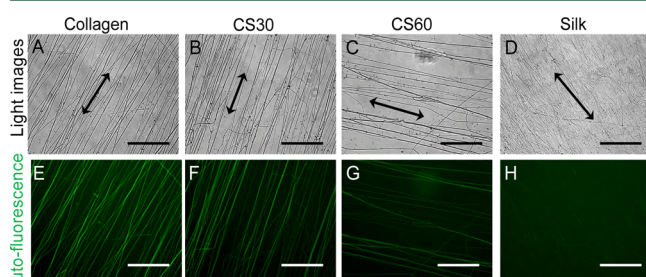


**Figure 1.** Bright field and autofluorescence images illustrating aligned E-spun fibers. Collagen (A, E), CS30 (B, F), CS60 (C, G), and silk (D, H) represent fibers with 0, 30, 60, and 100% (w/w) silk in collagen, respectively. The black arrows indicate the direction of fiber alignment. Bar size: 100  $\mu\text{m}$ .

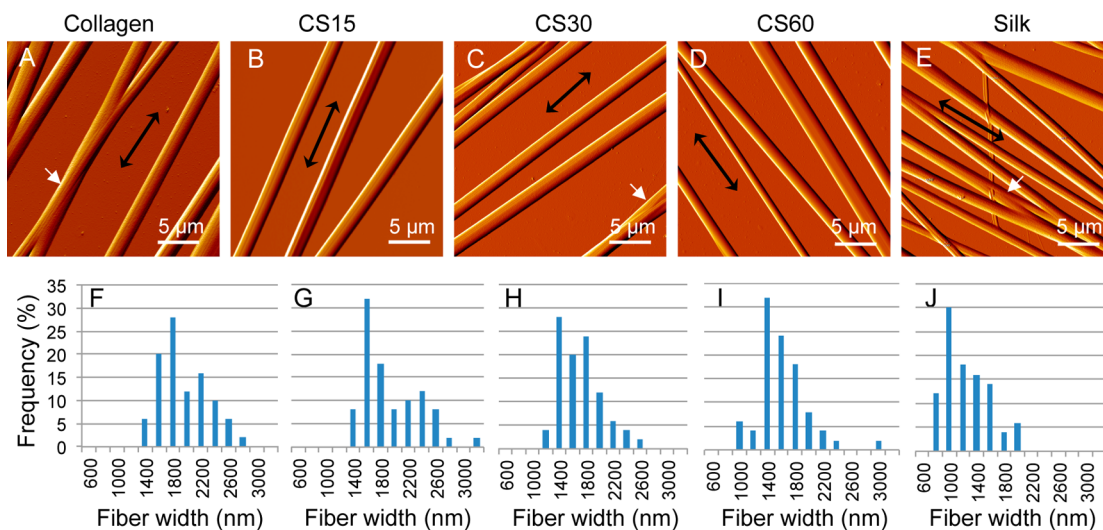


**Figure 2.** (A–E) AFM images of collagen (A), CS15 (B), CS30 (C), CS60 (D), and silk (E) fibers illustrating the fiber morphology. The black arrows indicate the fiber orientation. The white arrows highlight the splay fibers. (F–J) Fiber width distribution of the five fiber types. The width was measured from AFM images of 20–30 fibers per sample and more than 20 samples for each type of fibers.

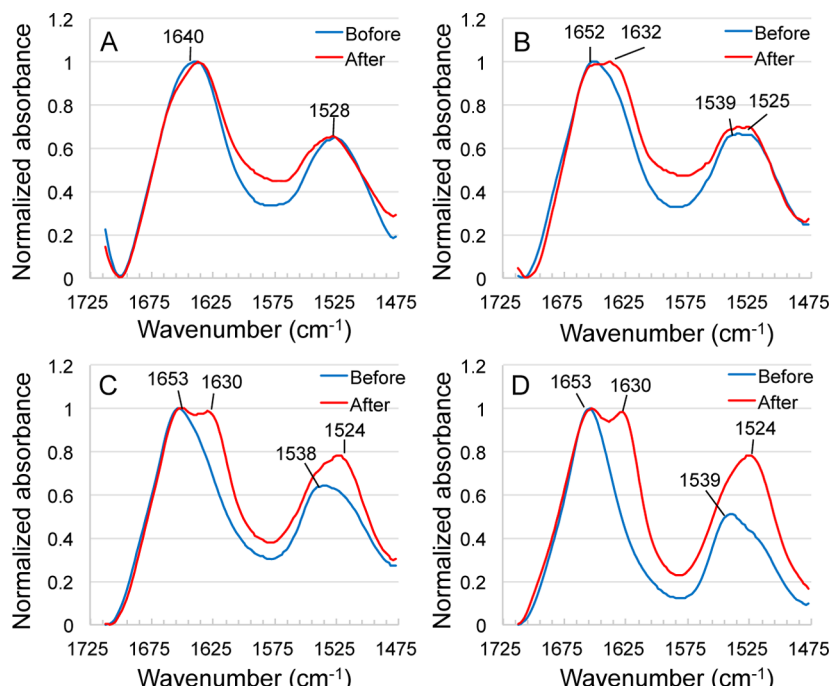


**Figure 3.** Normalized FTIR spectra of E-spun collagen–silk fibers before (blue) and after (red) glutaraldehyde vapor treatment: (A) pure collagen, (B) CS30, (C) CS60, and (D) pure silk.

autofluorescence images of pure collagen fibers, collagen-silk composite fibers with 30% silk (CS30) and 60% silk protein (CS60), and pure silk fibers. The intensity of collagen autofluorescence is uniform within each fiber and decreases in accordance with the reduction of collagen percentage (12.2, 8.5, 4.8, and 1.8 au for collagen, CS30, CS60, and silk, respectively). This suggests a homogeneous blending of collagen and silk protein at all ratios in a composite fiber. We also performed immunofluorescence staining for collagen type I and obtained similar results (see Figure S3), confirming the homogeneous integration between silk and collagen in the fibers. Silk fibers showed less alignment than collagen and collagen-composite fibers, likely due to the lower viscosity of the silk protein solution.

Figure 2A–E shows AFM images of fibers of pure collagen, CS15, CS30, CS60, and pure silk. At a fixed total protein concentration of 100 mg/mL, with the increase in silk protein percentage, the fiber density increases, accompanied by a decrease in fiber width. Fiber width and width distribution of the five fiber types are summarized in Figure 2F–J. All fibers, regardless of the fiber type, exhibit uniform width along a fiber, and each type of fiber has a narrow width distribution. Fibers with a narrow width distribution are desirable, as they offer comparable morphological cues from individual fibers to support collective cell development. Splay fibers were occasionally observed for each fiber type. The occurrence is attributed to the split of the primary jet during its traveling from the needle tip to the collector.<sup>37,38</sup>

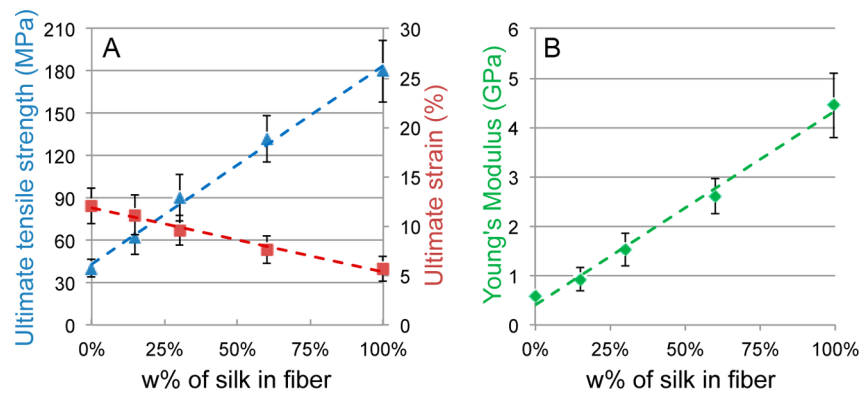


**Figure 4.** Variation of biomechanical properties with silk percentage in E-spun fibers. (A) Variation in ultimate tensile strength (blue) and ultimate strain (red); (B) variation in Young's modulus (green). The dashed lines represent the linear fitting of the experimental data. Error bars indicate standard deviation.

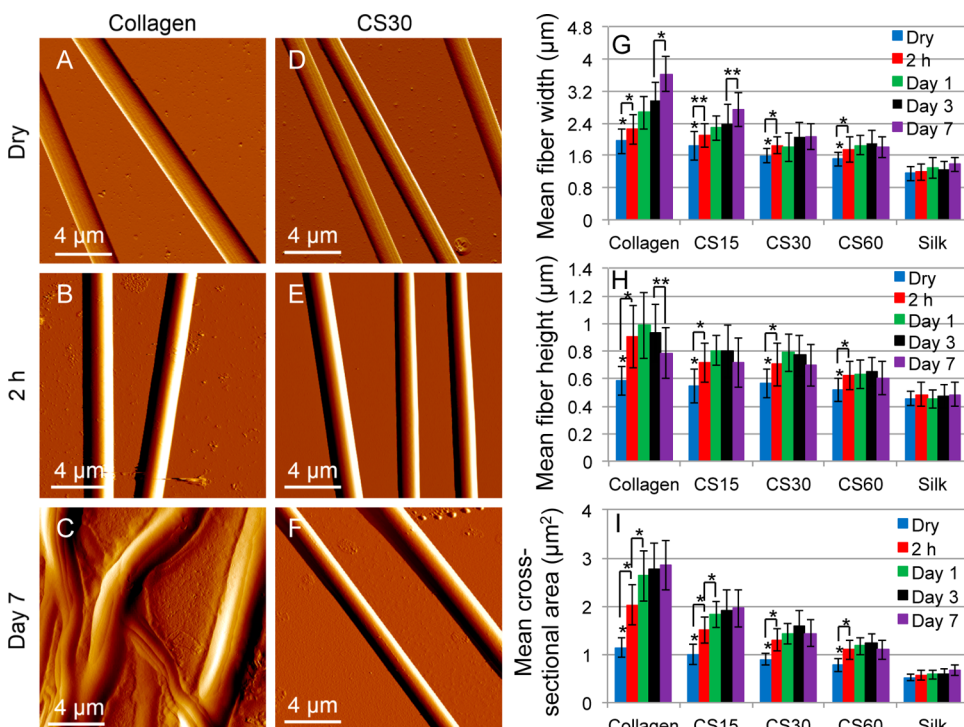


**Figure 5.** Fiber stability characterized by AFM. (A–C) AFM images of E-spun collagen fibers before (A) and after 2 h (B) and 7 days (C) of incubation in cell culture medium. (D–F) AFM images of E-spun CS30 fibers before (A) and after 2 h (B) and 7 days (C) of incubation in cell culture medium. (G–I) Mean fiber width (G), height (H), and cross-sectional area (I) of the five fiber types derived from AFM images collected at 0 to 7 days incubation in cell culture medium. Error bars indicate standard deviation. Statistical analysis: dry fibers, \* $p < 0.01$  vs pure silk fibers; pairwise comparison: \* $p < 0.01$  and \*\* $p < 0.05$ .

Light cross-linking was applied by glutaraldehyde vapor treatment to stabilize the fibers and to induce the formation of  $\beta$ -sheet of silk proteins.<sup>25,39</sup> Changes in the secondary structure of silk proteins before and after cross-linking the E-spun fibers were characterized by FTIR spectra at the amide I and amide II regions. The amide I band is mainly associated with the stretching vibrations of the carbonyl group along the polypeptide backbone and is a sensitive marker for the secondary structure of proteins.<sup>40,41</sup> As shown in Figure 3, for pure collagen fibers, amide I and amide II bands are centered at 1640 and 1528 cm<sup>-1</sup>, respectively, and are essentially unchanged after the treatment. The 1640 cm<sup>-1</sup> band is characteristic of the triple helix of native collagen.<sup>42–45</sup>

Its presence suggests the existence of the triple helical

structures in the E-spun fibers. In silk incorporated fibers (CS30, CS60, and pure silk), amide I and amide II bands appear at  $\sim$ 1653 and  $\sim$ 1539 cm<sup>-1</sup> before the cross-linking, suggesting a dominant random coil conformation of silk proteins;<sup>46,47</sup> however, shoulder peaks of 1630 and 1524 cm<sup>-1</sup> appear after the cross-linking, and they become more intense with the increase of silk percentage in the composite fibers. The FTIR peaks at 1630 and 1524 cm<sup>-1</sup> are characteristic of  $\beta$ -sheet conformation in silk proteins.<sup>48–50</sup> The FTIR spectrum of native dragline silk of *N. clavipes* was also collected, and it showed similar spectral features of the amide I and amide II bands as those of cross-linked E-spun silk fibers (Figure S4). The results suggest that the glutaraldehyde vapor treatment of E-spun fibers induced an apparent secondary structural

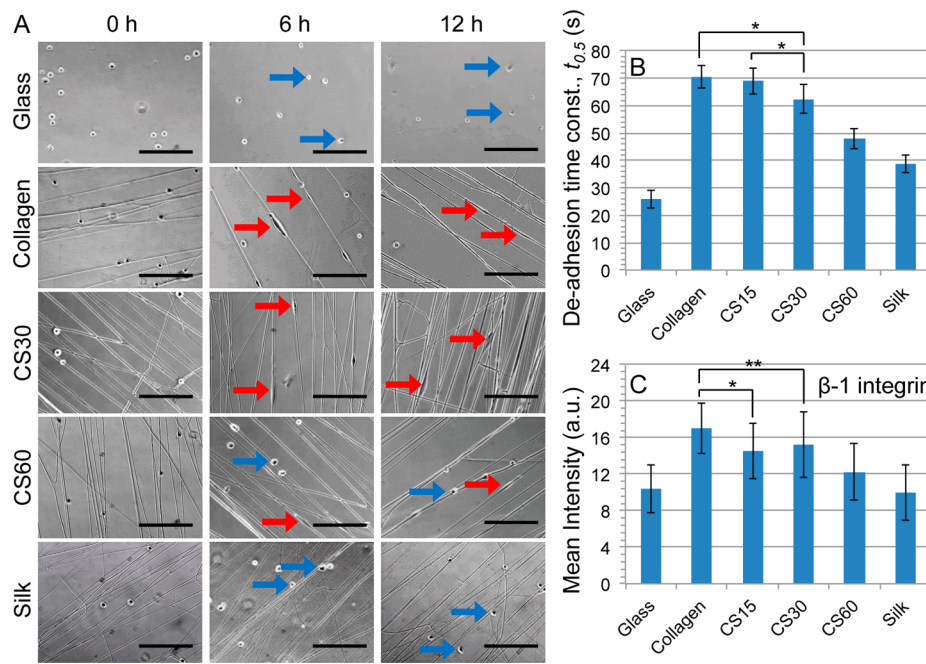


**Figure 6.** Characterization of cell adhesion to various matrices. (A) Change in hdpPSCs morphology on various matrices at 0, 6, and 12 h post-plating. The red and blue arrows indicate the elongated and rounded cells, respectively. (B) De-adhesion time constant ( $t_{0.5}$ ) at 12 h post-plating evaluated by a trypsin de-adhesion assay. (C) Mean intensity of  $\beta$ -1 integrin expression in cells at 12 h post-plating, derived from immunofluorescent images. Bar size: 100  $\mu$ m. Pairwise comparison: \* $p$  < 0.01 and \*\* $p$  < 0.05.  $p$  > 0.1 for de-adhesion time between collagen and CS15. Error bars indicate standard deviation.

transition from a random coil conformation to a  $\beta$ -sheet conformation of silk proteins. It is anticipated that the  $\beta$ -sheet structure of silk will enhance the mechanical strength of collagen–silk composite fibers.

The mechanical properties of E-spun fibers were characterized by stress–strain tests. As shown in Figure 4, both the ultimate tensile strength and the Young's modulus increased monotonically with silk percentage, ranging from 40 to 182 MPa and from 0.58 to 4.45 GPa, respectively. Meanwhile, the stretchability (ultimate strain) declined slightly from 12.1% for pure collagen to 5.6% for pure silk proteins. Evidently, the incorporation of silk greatly enhanced the mechanical strength of the collagen fibers, and the mechanical properties can be tuned in a marked range in a silk concentration-dependent manner.

To be used as a tissue-engineering scaffold, a matrix must remain stable in cell culture medium over a sufficiently long period of time. To characterize fiber stability, we monitored the changes in fiber morphology after incubation of the fibers in cell culture medium from 2 h to 7 days. As shown in the AFM images in Figure 5, dry fibers of different types had similar height but different width. A 2 h incubation in medium resulted in dramatic changes in all types of fibers. The mean cross-sectional area of pure collagen fibers increased by 80%, whereas the increases were much less in other fiber types: 49% for CS15, 44% for CS30, 41% for CS60, and 9.6% for pure silk. While both the width increase and the height increase were accountable for the increase in the fiber cross-sectional area, the increase in fiber height was more dramatic. Presumably, the dry fibers were relatively flat on the support substrates. A 2 h incubation in medium caused the fibers to swell when they took up water, and the expansion in the direction perpendicular to the substrate is more energetically favorable than a horizontal expansion due to the adhesion between the fiber and the

substrate. We observed a rapid increase in fiber cross-sectional area until day 1, and the change became negligible on days 3 and 7 in all types of fibers ( $p$  > 0.1). Interestingly, while the cross-sectional area of pure collagen fibers barely changed from days 3 to 7 ( $p$  > 0.1), the fiber width increased by 21.7% ( $p$  < 0.01), whereas the height dropped by 21.5% ( $p$  < 0.05). Meanwhile, most pure collagen fibers at day 7 curled and differed significantly from the orderly aligned straight and smooth fiber morphology (Figure 5C). In composite fibers and pure silk fibers, however, variations in fiber width, height, and cross-sectional area were less significant within the same time frame, and the fibers retained well-aligned and straight fiber morphology with only slight variations (Figure 5F). Thus, the integration of collagen with silk greatly enhanced the fiber stability and the composite fibers displayed better dissolution resistance against the aqueous cell culture system.

**Cell Adhesion to Composite Fibers.** Matrix adhesion is essential for cell attachment. It plays an important role in regulating cell differentiation. By optical imaging, we monitored the attachment of hdpPSCs on the E-spun fibers in the initial 12 h of culture. As shown in Figure 6A, on collagen-dominant matrices, most hdpPSCs promptly adhered to and spread along E-spun fibers within 6 h post-plating. On a glass substrate and silk protein-dominant matrices, however, most hdpPSCs retained a rounded shape even at 12 h post-plating. By day 1 (data not shown), hdpPSCs on glass, CS60, and silk matrices showed a lower cell density and smaller cell areas than those on collagen, CS15, and CS30 matrices. The results imply that cell attachment to silk is weaker than to collagen.

In order to evaluate the strength of cell–matrix adhesion on various E-spun fibers, a trypsin de-adhesion assay was carried out for cells at 12 h post-plating. Upon trypsinization, cells shrank over time until the steady, equilibrium state was reached (Figure S5). The time constant,  $t_{0.5}$ , was derived from a time-

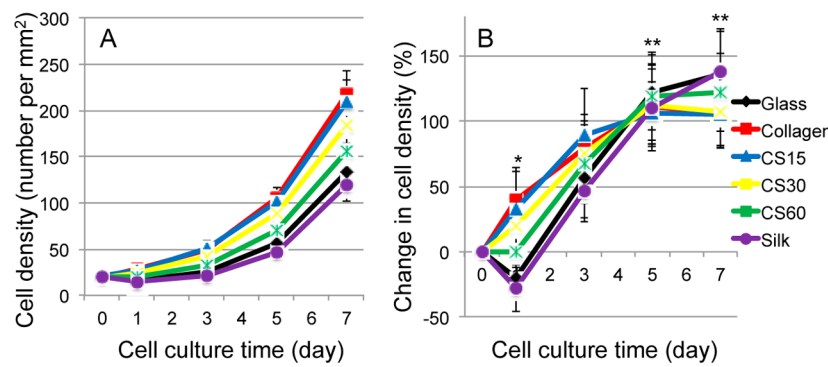


**Figure 7.** Characterization of hdpPSC proliferation on various matrices. (A) Increase in cell density with culture time; (B) change in cell density with time derived from panel A. The cell number per unit area was counted on the basis of DAPI staining on more than 20 images for each matrix type at each time point. Statistical analysis: \* $p < 0.01$  for collagen, CS15, and CS30 vs glass on day 1; \* $p < 0.05$  for CS60 vs glass on day 1; \*\* $p > 0.1$  for all matrices vs glass on days 5 and 7. Error bars indicate standard deviation.

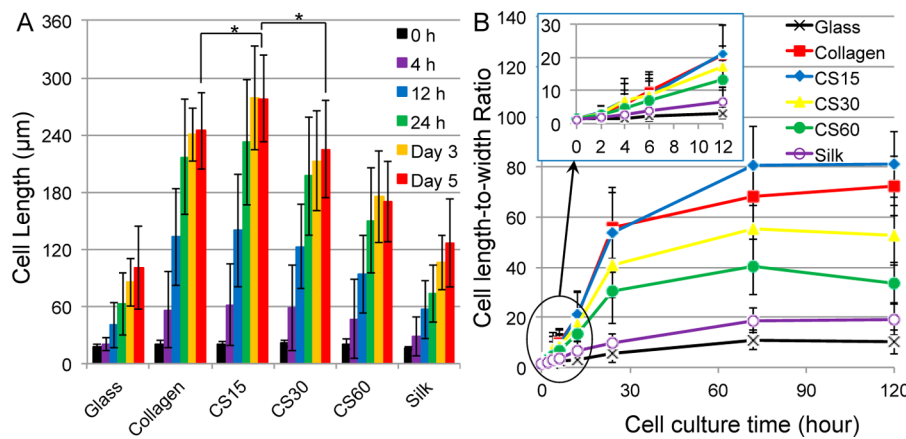


**Figure 8.** Characterization of cell polarization on various matrices. (A) Cell length was measured from bright-field images collected on various matrices at different time points. By day 5 of differentiation, the mean cell length for cells on CS15 is significantly longer than that on both collagen and CS30 (\* $p < 0.01$ ). (B) Cell length-to-width ratio was derived from the cell length and the cell area for cells grown on each type of fiber and at each time point. The inset in panel B highlights the cell polarization in the initial 12 h of culture. Error bars indicate standard deviation.

dependent de-adhesion curve to quantify the strength of cell adhesion. As shown in Figure 6B, the time constant is much longer on collagen, CS15, and CS30 than on CS60, silk, and glass, implying slower detachment processes and consequently stronger cell adhesion on the collagen-dominant matrices. This is consistent with the observations in Figure 6A.

Considering that  $\beta$ -1 integrin is the collagen type I binding receptor on cell membranes and mediates cell–matrix adhesion, we quantified the  $\beta$ -1 integrin expression level in cells on various matrices at 12 h post-plating (Figure 6C). In agreement with the result of trypsin de-adhesion assay, higher expression levels of  $\beta$ -1 integrin were observed in cells on collagen and collagen-dominant matrices, whereas the expression level dropped with the collagen percentage in composite fibers. Thus, cells responded to the matrix composition by secreting different levels of  $\beta$ -1 integrin, which is attributable to the variation in cell–matrix adhesion. One exception was that cells on CS15 showed a decreased level of  $\beta$ -1 integrin expression ( $p < 0.01$ ) but a similar level of cell adhesion ( $p > 0.1$ ) as compared to that of cells on pure collagen. This is associated with the higher level of cell polarization and the development of longer filaments on CS15 (to be delineated in the Discussion section).

### Cell Proliferation and Polarization on Composite Fibers.

Cell proliferation was profiled on various matrices. As

shown in Figure 7, the cell density is higher on collagen-dominant matrices than on the control and silk protein-dominant matrices over the entire period of time for cell culture. By day 1, the cell density on collagen, CS15, and CS30 increased by 40, 32, and 18%, respectively, but remained nearly constant on CS60 and decreased by 20 and 28% on glass and silk matrices, respectively. Later, the rate of cell proliferation increased on all matrices. By day 5, the proliferation rate plateaued on collagen and collagen-silk composite matrices, whereas on glass and silk, it kept increasing until day 7. When the growth rate was evaluated in the logarithmic phase, the doubling time of hdpPSCs was found to range narrowly between 39 and 47 h for cells on various matrices. This implies that all five fiber types support cell proliferation at a similar rate and that the difference in matrix adhesion is attributed to the difference in initial cell density on various matrices.

With the unidirectionally aligned fibers, cells were polarized along the fibers (Figure 6A). At 6 h post-plating, most of the cells on collagen, CS15, and CS30 fibers showed a spindle shape. By 12 h, these cells elongated along the E-spun fibers and developed a bipolar neuro-epithelial like morphology. By day 1, the cells further polarized and displayed small cell bodies and long filaments along the aligned fibers. On CS60 and silk matrices, cells polarized less and more slowly; about half of the cells retained a rounded shape until 8 h (CS60) and 24 h (silk)

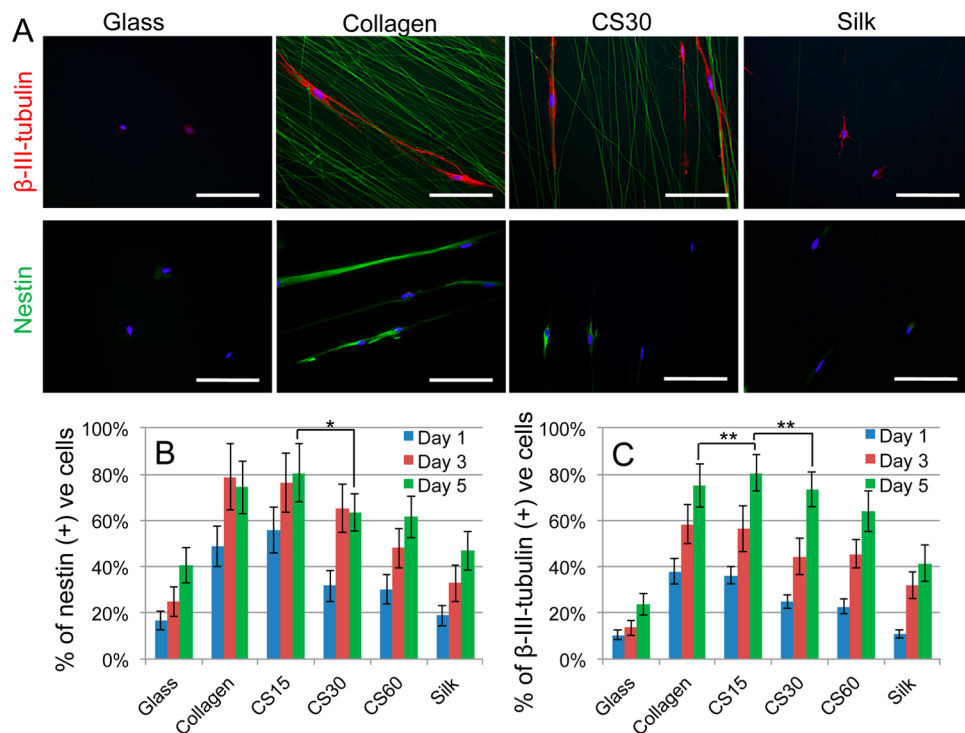


**Figure 9.** hdpPSC differentiation profile on various matrices. (A) Immunofluorescent images showing β-III-tubulin positive cells (red) and nestin positive cells (green) at day 1 of differentiation. DAPI staining (blue) illustrates the nuclei of cells. The auto-fluorescence of collagen (green) is shown in β-III-tubulin (red) staining images to illustrate the relative location between cells and the fibers. Bar size: 100 μm. (B, C) Percentage of nestin positive cells (B) and β-III-tubulin positive cells (C) on various matrices at days 1, 3, and 5 of differentiation. Pairwise comparison: \* $p < 0.01$  and \*\* $p < 0.05$ . Error bars indicate standard deviation.

post-plating. Cells grown on glass displayed a rounded shape until 6 h post-plating. They developed polygonal cell morphologies and spread along random directions in a longer term of culture.

Cell polarization was quantified by measuring the length and the projection area of cells using the ImageJ software. As shown in Figure 8A, the mean cell length of irregularly shaped cells on a glass substrate is 62 μm after 24 h of cell culture. On a collagen matrix, most cells started to elongate within 2 h post-plating and developed long filaments along the fiber by 24 h (a mean cell length of 226 μm). On CS15 and CS30, cells elongated as fast as those on collagen. By day 5, the length of cells on CS15 exceeded those on any other matrices, and some cells displayed filaments as long as 345 μm. On silk-dominant matrices (CS60 and silk), cells started to spread earlier than on glass substrates, but the cells did not grow as long as those on collagen, CS15 and CS30. Cell polarization is better characterized by the cell length-to-width ratio, and the calculated results are shown in Figure 8B. The ratio increases rapidly in the first 24 h of culture on collagen, CS15, CS30, and CS60 and continuously increases at a reduced rate until day 3. The highest length-to-width ratio was obtained on CS15 at day 3, which is 20% higher than the ratio on pure collagen at the same time point ( $p < 0.01$ ). After day 3, no statistically significant changes were observed. The length-to-width ratio of cells on pure silk was remarkably lower than that on collagen and composite fibers, but it is higher than that on glass. These results suggest that all of the E-spun composite fibers promoted cell polarization, albeit to a different extent, and that cells grown on the composite fibers experienced an earlier and faster polarization than those on pure silk and glass substrates. CS15

surpassed the performance of any other fiber type and induced the extended 1D development of cell filaments.

**Matrix Directed Neural Differentiation.** Collagen type I is known to support neural differentiation of stem cells. The aligned matrices provide the combined biophysical and biochemical cues for cell polarization and differentiation and are expected to promote neural differentiation of stem cells. Nestin is an intermediate filament protein and is expressed at a high level by neural precursors.<sup>51</sup> β-III tubulin is a neuron-specific isoform expressed by immature neurons and outgrowth neurites.<sup>52</sup> Expressions of nestin and β-III tubulin were examined to investigate the neural commitment and further differentiation of hdpPSCs on various matrices (Figure 9). The bipolar-shaped cells on collagen-dominant matrices expressed nestin at a higher level than that of the polygonal-shaped cells on glass and silk. Note that the auto-fluorescence of collagen (green) is negligible when compared with the strong fluorescence from the secondary antibody; thus, it fell below the background level in the characterization of nestin expression (green). β-III tubulin expression (red) demonstrated a similar pattern. The long filaments of cells are shown to match the aligned fibers exactly, as illustrated by the auto-fluorescence of collagen that was intentionally adjusted to be visible in this case. The expression levels of both nestin and β-III tubulin showed similar profiles as that of the mean cell length (Figure 8A). Notably, while the β-III tubulin expression level increased with time on all matrices, the increase of nestin expression on collagen, CS15, and CS30 stalled by day 3. This suggests that hdpPSCs on these matrices have committed to neural lineage and that they more rapidly transited to progenitor phenotypes than did cells on CS60, silk, and the control glass substrates.

Neural progenitors have the ability to further differentiate toward more mature neural cells. The expression of NeuN, a marker of neural progenitors and mature neurons,<sup>53</sup> was examined at days 1, 3, and 5 of differentiation (Figure 10). At

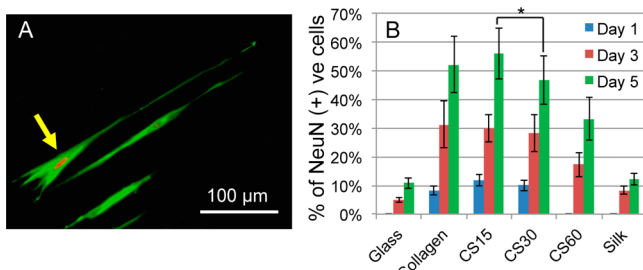


**Figure 10.** hdpPSC maturation on various matrices by day 5 of differentiation. (A) Immunofluorescent images illustrating NeuN (red) positive cells co-staining with nestin (green) on CS15 matrix at day 3 of differentiation. The yellow arrow demonstrates a cell with the typical neural progenitor cell shape, revealing a long filament, a small cell body, and dendrites. (B) ImageJ quantification of the percentage of NeuN positive cells at days 1, 3, and 5 of differentiation. *t*-test analysis revealed that the difference in NeuN expression for cells on CS15 and CS30 is significant ( $p < 0.05$ ); the difference for cells on collagen and CS15 is moderately significant ( $p < 0.1$ ). Error bars indicate standard deviation.

day 1, only on collagen, CS15, and CS30 were we able to observe a few positively stained cells. NeuN-positive cells were observed on all types of matrices by day 3 of differentiation, and the percentage of positive cells continuously increased over the 5 days of cell culture. By day 5, the percentage of NeuN positive cells was 53, 56, 47, 33, 13, and 12% on pure collagen, CS15, CS30, CS60, silk, and glass, respectively. The result suggests that by day 5 more cells on collagen, CS15, and CS30 developed into mature neural cells, while cells on other matrices lagged behind. CS15 promoted neural differentiation at the same or slightly higher level when compared to that on pure collagen and CS30, and it outperformed any other matrices in inducing the development of long neural filaments.

## DISCUSSION

In this work, we produced collagen–silk composite fibers by electrospinning, studied their mechanical properties, and applied them as aligned matrices for neural differentiation. The two protein components, collagen type I and spider dragline silk proteins, are building blocks of natural biopolymers and have distinct structures and complementary properties.<sup>23</sup> Collagen type I has a hierarchical structure, and its monomer (tropocollagen), comprised of triple  $\alpha$  helices, is hydrophilic and binds to  $\beta$ -1 integrin on a cell membrane.<sup>54,55</sup> Dragline silk proteins, consisting of predominantly  $\beta$ -sheets and glycine-rich domains (amorphous matrix), have impressive mechanical properties and are relatively hydrophobic.<sup>19</sup> The secondary structures of the proteins were largely retained in the E-spun fibers. As expected, collagen–silk composite fibers exhibited physical and biochemical properties that were contributed by both protein components.

**Fiber Mechanics and Stability.** High mechanical strength is essential for fibers to be manually manipulated when serving as scaffolds for tissue engineering.<sup>56</sup> Under the optimized electrospinning conditions in this study, E-spun fibers of pure collagen had a mean ultimate tensile strength, elastic modulus,

and ultimate strain of 40 MPa, 0.58 GPa, and 12.1%, respectively, whereas the corresponding values of silk fibers were 182 MPa, 4.45 GPa, and 5.6%. Thus, silk fibers are stronger and stiffer, whereas collagen fibers are slightly more stretchable. The monotonic and progressive increase in fiber mechanical properties with silk percentage (Figure 4) indicates the effectiveness of silk proteins in improving collagen fiber mechanics. It also suggests a homogeneous integration between collagen and silk protein without abrupt structural changes in the entire ratio range, and the composite fibers render tunable fiber strength to achieve resistance to both fracture and rupture. Note that E-spun fibers have lower tensile strength, stiffness, and stretchability than that of native protein fibers (120 MPa, 1.2 GPa and 13% for collagen in tendon;<sup>22,23</sup> 1.1 GPa, 22 GPa, and 10–35% for dragline silk<sup>20,21</sup>) despite the presence of  $\beta$ -sheets of silk proteins and triple helix of collagen in the E-spun fibers. We attribute this discrepancy to imperfect molecular assembly during the electrospinning process; however, when seeking a remarkably efficient and inexpensive way to fabricate aligned and freestanding matrices, the E-spun collagen–silk fibers offer an advantage for practical tissue engineering applications. Efforts have been made to develop protocols for effective post-treatments of artificial silk fibers<sup>20,57,58</sup> to induce  $\beta$ -sheet alignments, and similar treatments can be applied to E-spun fibers in order to further improve the fiber mechanics.

Preserving matrix stability is critical, as it enables cells to receive steady biophysical and biochemical signals for directing cell fate decisions.<sup>3,59,60</sup> Collagen fibers were shown to change dramatically in fiber dimension and fiber morphology upon 7 days incubation in cell culture medium (Figure 5). Hydration of collagen is the major cause of the change. Due to the high percentage of hydrophilic amino acids in collagen, uncross-linked collagen hydrogel was reported to swell 150–200 wt %.<sup>61</sup> In native fibers, selected lysine cross-linking sites can minimize the distance between neighboring molecules,<sup>62</sup> enhancing the hydrogen bonding and electrostatic interactions, which play important roles in sustaining fiber stability.<sup>63</sup> We applied a glutaraldehyde vapor treatment for cross-linking. While a pronounced effect on fiber mechanics and stability was observed (to be reported separately), the random and nonselective bonding may be insufficient, and the slow penetration of glutaraldehyde makes the cross-linking less effective on protein molecules within a fiber.<sup>64</sup> This is supported by our observation that the glutaraldehyde cross-linking stabilizes thinner fibers more effectively. During the hydration process, water molecules likely bind to the uncross-linked hydrophilic residues of collagen. This causes an initial increase in the fiber volume (first 2 h). When the water uptake becomes excessive (after 7 days), it disturbs the hydrogen-bonding network within a fiber. Consequently, the dense molecular packing within a fiber collapses, leading to a looser fiber characterized by a significantly increased cross-sectional area<sup>65</sup> and a distorted fiber morphology. Silk protein is more hydrophobic and takes up much less water than collagen. In composite fibers, not only does the increase of silk percentage effectively reduce the water uptake but also the hydrogen bonding and molecular interaction between the two protein components reduce the degree of water uptake.<sup>17</sup> Consistently, our results demonstrate that the incorporation of silk protein dramatically improved fiber stability. At day 7, a 15, 30, and 60% silk protein incorporation effectively reduced the collagen fiber swelling from 150.3% to 95.3, 60.1, and 40.1%, respectively, and the fibers largely retained the well-aligned,

straight fiber morphology. The cross-sectional area of pure silk fibers increased by only 28.0% after incubation in medium for 7 days, and the fiber morphology remained unchanged. When the fiber integrity is retained, the fiber stiffness is sustained. Cognate changes in fiber stiffness were observed along with fiber swelling. The integration of collagen with silk resulted in a less noticeable decrease in fiber stiffness (see Figure S6). Thus, silk-dominant fibers offer mechanically stronger and more stable scaffolds than that of pure collagen and collagen-dominant fibers.

**Biocompatibility and Application in Stem Cell Differentiation.** hdpPSCs behave very differently on various E-spun matrices. Collagen-dominant fibers are more favorable for hdpPSCs attachment. While the hydrophobicity of silk hampers the initial cell attachment on silk-dominant fibers, cells eventually adapt to the matrix and proliferate at a similar rate as that of cells on collagen-dominant fibers. Cells on glass and silk-dominant matrices seem to proliferate at a higher rate by day 7. This is mainly because a larger fraction of cells on collagen-dominant matrices have stopped self-renewal while progressing toward neural differentiation.

A cell responds to matrix by modulating the amount and distribution of matrix-binding membrane proteins and reshaping the cytoskeleton structure. The specific cell surface receptor of collagen,  $\beta$ -1 integrin, is the key protein for sensing and transmitting the physical and chemical cues of the matrix for intracellular signaling. The unidirectionally aligned collagen molecules in an E-spun composite fiber provide the guidance for  $\beta$ -1 integrin deposition, and the formed  $\beta$ -1 integrin–collagen complexes induce cell polarization along the fibers. Cells grown on composite fibers with a higher collagen percentage display stronger adhesion with a concomitant higher expression of  $\beta$ -1 integrin (Figure 6), as expected. One exception was found on CS15, where hdpPSCs expressed  $\beta$ -1 integrin at a lower density (characterized by the reduced intensity of fluorescence signal) as compared to that of cells on pure collagen; however, the cell adhesion strength (characterized by  $t_{0.5}$ ) was similar on the two matrices. The reduced density of  $\beta$ -1 integrin is partly due to the reduced amount of collagen in the composite fiber, which downregulates  $\beta$ -1 integrin expression. It can also be ascribed to the greater level of cell polarization on CS15, which demands and drives  $\beta$ -1 integrin to be distributed over a stretched range. The broader distribution of  $\beta$ -1 integrin across the elongated cell appeared to compensate the reduced protein density and dominate the enhancement of overall cell adhesion. Cell spreading involves the breaking up of existing integrin–collagen binding complexes, the translocation of integrin to new binding sites, and the establishment of new binding complexes. Therefore, slightly reduced  $\beta$ -1 integrin expression (i.e., reduced number of collagen–integrin binding complexes) requires less energy for cell spreading and favors cell polarization and the development of long filaments.

Fibrillar collagen type I has been routinely used as a matrix component in culturing neural stem cells or neural progenitors due to integrin-mediated intracellular signaling.<sup>3,7,66,67</sup> Our previous work has shown that the neural differentiation of stem cells on a collagen gel-coated substrate is attributed to a  $\beta$ -1 integrin mediated  $\beta$ -catenin signaling pathway.<sup>9</sup> In this well-studied signaling pathway, the binding of  $\beta$ -1 integrin to collagen stimulates integrin-linked kinase (ILK). ILK causes the repression of E-cadherin, leading to the nuclear accumulation of  $\beta$ -catenin,<sup>68,69</sup> which, in turn, induces expression of genes

whose protein products are associated with neural commitment.<sup>51</sup> Neural precursors express nestin at a high level. By day 1 of differentiation, 48% of cells on pure collagen and 56% of cells on CS15 were already nestin-positive (Figure 9B), implying a fast neural commitment of hdpPSCs on these matrices. During further neural differentiation, nestin is normally downregulated and is replaced by tissue-specific neurofilament proteins;<sup>70</sup> however, we found that the nestin expression level in cells on collagen-dominant matrices were steady and remained high from days 3 to 5 of differentiation. We ascribe this to nestin's other function, that is, coordinating the assembly and disassembly of intermediate filaments as well as the organization and maintenance of polarized cell morphology.<sup>71</sup> This is evidenced by the striking similarity in the profiles of the nestin expression level and the cell length of hdpPSCs on various matrices (Figures 8A and 9B).

Transition of the neural progenitors to more mature neural cells was characterized by the expressions of  $\beta$ -III tubulin and NeuN, markers for immature and mature neurons, respectively. We achieved the highest percentage of NeuN-positive cells (55%) on CS15 at day 5. On the same matrix, we achieved the highest percentage of  $\beta$ -III tubulin-positive cells at 86%. A longer term of culture in the spontaneous differentiation medium did not trigger a higher level of NeuN expression. We infer that while most hdpPSCs can differentiate and transition to neural progenitors and immature neural cells only a portion can mature further. This result suggests that pro-neural soluble factors, such as neural growth factors or retinoic acid (RA), are required to advance further differentiation and maturation.

It is remarkable that CS15 promoted the neural differentiation at the same or a slightly higher level compared with that of pure collagen even though  $\beta$ -1 integrin expression in cells on CS15 is lower. We speculate that, in addition to the  $\beta$ -1 integrin-dependent pathway, there may be other signaling pathways that elevate the neural differentiation of hdpPSCs on CS15 fibers. Many reports have shown that the organization, composition, and presentation of ligands exhibited by the extracellular matrix can direct stem cell differentiation.<sup>72,73</sup> As discussed earlier, silk proteins in a CS15 fiber dilute the distribution density of collagen, causing the downregulation of  $\beta$ -1 integrin expression and a subsequent reduction in the number of focal adhesion complexes, thereby leading to a higher level of cell polarization. The enhanced cell polarization is expected to affect actomyosin contractility and the downstream integrin-linked signaling cascades to promote neural differentiation. This is supported by the fact that, when compared with hdpPSCs differentiation on collagen gel (with randomly oriented fibers), cells on E-spun collagen fibers were highly polarized and experienced a much earlier  $\beta$ -III tubulin expression, suggesting a faster neural differentiation (1 day vs 3 days). On the other hand, the incorporation of silk into collagen increased the fiber stiffness (Figure S6). Studies have shown that a stiffer matrix can induce tensional forces, causing the cell–matrix adhesion proteins to trigger a mechanotransductive pathway.<sup>6,9,74,75</sup> Thus, we infer that the effect from the drop of  $\beta$ -1 integrin expression, associated with the reduced number of collagen molecules in a composite fiber, is counterbalanced to some extent by the effect of the extensive cell polarization and increased fiber stiffness; however, a further decrease of collagen percentage in composite fibers (CS30 and CS60) did not lead to further augmentation of hdpPSC differentiation despite the continuous increase in matrix stiffness. These results suggest that a fine balance between

the physical and biochemical cues is imperative to achieve rapid and effective neural differentiation. More studies must be undertaken to identify the signaling pathway mediated by the unique fiber composition. Not only will the number of collagen–integrin binding sites be examined within a composite fiber but also the cell adhesion strength of each binding site will also be quantified to further understand the role of cell–matrix interaction in promoting hdpPSC differentiation.

Implantation devices for neural tissue engineering, such as neural constructs/scaffolds and neural electrodes, are typically on the millimeter scale.<sup>76–78</sup> Accordingly, a fiber length of 8–10 mm was chosen in this study. With the current setup of the electrospinning system, aligned fibers up to 2 cm long can be achieved by adjusting the spin conditions. Longer fibers can be generated at the expense of fiber alignment and desirable properties, such as dimension, distribution, and mechanical strength. Thus, alternative methods are preferable for generating longer fibers in other applications.

A low fiber density was chosen in this study to promote cell attachment to an individual fiber for effective cell polarization and differentiation and to induce the development of long neural filaments in a desired direction. Potentially, layer-by-layer E-spun fiber scaffolds with controllable architectures can be achieved, serving as a 3D matrix for generating biocircuits from stem cells.

## CONCLUSIONS

Artificial extracellular matrices with tunable properties and spatial alignment can serve as promising tissue engineering scaffolds. In this study, we successfully fabricated unidirectionally aligned, freestanding collagen–silk composite fibers by electrospinning. To our knowledge, this research is the first work to fabricate collagen–dragline silk composite fibers. The use of the electrospinning method is beneficial, as it allows the formation of aligned fibers, mimicking interstitial ECM proteins that typically align in parallel arrays *in vivo*. Collagen and silk proteins were uniformly blended throughout the fibers, and their fiber tensile strength, strain, and elasticity displayed linear variation with the fiber composition, allowing a simple and convenient way to fine-tune the mechanical properties of a matrix by its chemical composition.

All of the E-spun fibers, including pure silk fibers, adequately supported cell proliferation. Due to the intrinsic difference between collagen and silk proteins, collagen-dominant fibers displayed better cell adhesion, whereas silk-dominant proteins displayed greater fiber stability. When the collagen percentage was tuned in the range of 0–100% in the E-spun fibers, the distribution density of ligand binding sites, cell polarity, and matrix stiffness were tuned in accordance. A fine balance between the biophysical and biochemical cues was achieved on the CS15 matrix to provide optimal support for the neural differentiation of hdpPSCs and, importantly, to develop extremely long neural filaments accurately aligned with the fibers, implying the potential application of this matrix in neural tissue repair and future nanobiodevices.

## ASSOCIATED CONTENT

### Supporting Information

Scheme of the home-built electrospinning system; cross-sectional profile for deriving the cross-sectional area of a fiber; immunofluorescent images of collagen type I in various E-spun fibers; normalized FTIR spectrum of native dragline silk fibers of *Nephila clavipes* in comparison with the spectra of E-

spun silk fibers before and after glutaraldehyde vapor treatment; characterization of cell de-adhesion; Young's modulus of individual fibers before and after 7 days of fiber incubation in cell culture medium, characterized by a nanoindentation method. This material is available free of charge via the Internet at <http://pubs.acs.org>.

## AUTHOR INFORMATION

### Corresponding Author

\*E-mail: wangr@iit.edu. Fax: +1 312 567 3494. Tel.: +1 312 567 3121.

### Notes

The authors declare no competing financial interest.

## ACKNOWLEDGMENTS

We thank Russ Janota for his assistance in testing fiber mechanics. We also thank Dr. Zuzana Strakova at the University of Illinois in Chicago for providing the human decidua parietalis placental stem cells (hdpPSCs). This research was partly supported by NIH (R01 NS047719) and the Utah Science Technology and Research (USTAR) initiative fund.

## REFERENCES

- Hung, M. J.; Wen, M. C.; Hung, C. N.; Ho, E. S.; Chen, G. D.; Yang, V. C. *Int. Urogynecol. J.* **2010**, *21*, 1085–93.
- da Silva, E. E.; Della Colletta, H. H. M.; Ferlauto, A. S.; Moreira, R. L.; Resende, R. R.; Oliveira, S.; Kitten, G. T.; Lacerda, R. G.; Ladeira, L. O. *Nano Res.* **2009**, *2*, 462–73.
- Engler, A. J.; Sen, S.; Sweeney, H. L.; Discher, D. E. *Cell* **2006**, *126*, 677–89.
- Bosman, F. T.; Stamenkovic, I. *J. Pathol.* **2003**, *200*, 423–8.
- Grover, C. N.; Cameron, R. E.; Best, S. M. *J. Mech. Behav. Biomed. Mater.* **2012**, *10*, 62–74.
- Sridharan, I.; Kim, T.; Wang, R. *Biochem. Biophys. Res. Commun.* **2009**, *381*, 508–12.
- Lin, H. J.; O'Shaughnessy, T. J.; Kelly, J.; Ma, W. *Dev. Brain Res.* **2004**, *153*, 163–73.
- Ma, W.; Tavakoli, T.; Derby, E.; Serebryakova, Y.; Rao, M. S.; Mattson, M. P. *BMC Dev. Biol.* **2008**, *8*, 90.
- Sridharan, I.; Kim, T.; Strakova, Z.; Wang, R. *Biochem. Biophys. Res. Commun.* **2013**, *437*, 489–95.
- Li, W.; Zhu, B.; Strakova, Z.; Wang, R. *Biochem. Biophys. Res. Commun.* **2014**, *450*, 1377–82.
- Sridharan, I.; Ma, Y.; Kim, T.; Kobak, W.; Rotmensch, J.; Wang, R. *Biomaterials* **2012**, *33*, 1520–7.
- Friedrichs, J.; Taubenberger, A.; Franz, C. M.; Muller, D. J. *J. Mol. Biol.* **2007**, *372*, 594–607.
- Kirmse, R.; Otto, H.; Ludwig, T. *J. Cell Sci.* **2011**, *124*, 1857–66.
- Lee, Y. S.; Arinze, T. L. *Polymers* **2011**, *3*, 413–26.
- Ma, Z.; Kotaki, M.; Inai, R.; Ramakrishna, S. *Tissue Eng.* **2005**, *11*, 101–9.
- Shih, Y. R.; Chen, C. N.; Tsai, S. W.; Wang, Y. J.; Lee, O. K. *Stem Cells* **2006**, *24*, 2391–7.
- Lin, H. Y.; Kuo, Y. J.; Chang, S. H.; Ni, T. S. *Biomed. Mater.* **2013**, *8*, 025009.
- Rho, K. S.; Jeong, L.; Lee, G.; Seo, B. M.; Park, Y. J.; Hong, S. D.; Roh, S.; Cho, J. J.; Park, W. H.; Min, B. M. *Biomaterials* **2006**, *27*, 1452–61.
- van Beek, J. D.; Hess, S.; Vollrath, F.; Meier, B. H. *Proc. Natl. Acad. Sci. U.S.A.* **2002**, *99*, 10266–71.
- Teule, F.; Addison, B.; Cooper, A. R.; Ayon, J.; Henning, R. W.; Benmore, C. J.; Holland, G. P.; Yarger, J. L.; Lewis, R. V. *Biopolymers* **2012**, *97*, 418–31.
- Cunniff, P. M.; Fossey, S. A.; Auerbach, M. A.; Song, J. W.; Kaplan, D. L.; Adams, W. W.; Eby, R. K.; Mahoney, D.; Vezie, D. L. *Polym. Adv. Technol.* **1994**, *5*, 401–10.

- (22) Pollock, C. M.; Shadwick, R. E. *Am. J. Physiol.* **1994**, *266*, R1016–21.
- (23) Gosline, J.; Lillie, M.; Carrington, E.; Guerette, P.; Ortlepp, C.; Savage, K. *Philos. Trans. R. Soc., B* **2002**, *357*, 121–32.
- (24) An, B.; Jenkins, J. E.; Sampath, S.; Holland, G. P.; Hinman, M.; Yarger, J. L.; Lewis, R. *Biomacromolecules* **2012**, *13*, 3938–48.
- (25) Yeo, I. S.; Oh, J. E.; Jeong, L.; Lee, T. S.; Lee, S. J.; Park, W. H.; Min, B. M. *Biomacromolecules* **2008**, *9*, 1106–16.
- (26) Wang, G.; Hu, X.; Lin, W.; Dong, C.; Wu, H. *In Vitro Cell. Dev. Biol.: Anim.* **2011**, *47*, 234–40.
- (27) Ihnatovych, I.; Hu, W.; Martin, J. L.; Fazleabas, A. T.; de Lanerolle, P.; Strakova, Z. *Endocrinology* **2007**, *148*, 3176–84.
- (28) Strakova, Z.; Livak, M.; Krezalek, M.; Ihnatovych, I. *Cell Tissue Res.* **2008**, *332*, 479–88.
- (29) Ma, W.; Fitzgerald, W.; Liu, Q. Y.; O'Shaughnessy, T. J.; Maric, D.; Lin, H. J.; Alkon, D. L.; Barker, J. L. *Exp. Neurol.* **2004**, *190*, 276–88.
- (30) Tucker, C. L.; Jones, J. A.; Bringhurst, H. N.; Copeland, C. G.; Addison, J. B.; Weber, W. S.; Mou, Q.; Yarger, J. L.; Lewis, R. V. *Biomacromolecules* **2014**, *15*, 3158–70.
- (31) Beachley, V.; Wen, X. *Mater. Sci. Eng., C* **2009**, *29*, 663–8.
- (32) Li, D.; Wang, Y. L.; Xia, Y. N. *Nano Lett.* **2003**, *3*, 1167–71.
- (33) Dechant, J. *Acta Polym.* **1988**, *39*, 150.
- (34) Strakova, Z.; Livak, M.; Krezalek, M.; Ihnatovych, I. *Cell Tissue Res.* **2008**, *332*, 479–88.
- (35) Sen, S.; Kumar, S. *Cell. Mol. Bioeng.* **2009**, *2*, 218–30.
- (36) Tibbitt, M. W.; Kloxin, A. M.; Dyamenahalli, K. U.; Anseth, K. S. *Soft Matter* **2010**, *6*, 5100–8.
- (37) Deitzel, J. M.; Kleinmeyer, J.; Harris, D.; Tan, N. C. B. *Polymer* **2001**, *42*, 261–72.
- (38) Koombhongse, S.; Liu, W.; Reneker, D. H. *J. Polym. Sci., Part B: Polym. Phys.* **2001**, *39*, 2598–606.
- (39) Cui, X.; Liu, X.; Kong, D.; Gu, H. *IFMBE Proc.* **2013**, *39*, 79–82.
- (40) Payne, K. J.; Veis, A. *Biopolymers* **1988**, *27*, 1749–60.
- (41) Surewicz, W. K.; Mantsch, H. H. *Biochim. Biophys. Acta* **1988**, *952*, 115–30.
- (42) Kittipattanabawon, P.; Benjakul, S.; Visessanguan, W.; Shahidi, F. *Food Sci. Technol.* **2010**, *43*, 792–800.
- (43) Wehbe, K.; Pinneau, R.; Moenner, M.; Deleris, G.; Petibois, C. *Anal. Bioanal. Chem.* **2008**, *392*, 129–35.
- (44) Nagai, T.; Suzuki, N.; Tanoue, Y.; Kai, N.; Nagashima, T. *Food Nutr. Sci.* **2010**, *59*–66.
- (45) Hu, X.; Raja, W. K.; An, B.; Tokareva, O.; Cebe, P.; Kaplan, D. L. *Sci. Rep.* **2013**, *3*, 3428.
- (46) Kim, S. H.; Nam, Y. S.; Lee, T. S.; Park, W. H. *Polym. J.* **2003**, *35*, 185–90.
- (47) Bini, E.; Foo, C. W.; Huang, J.; Karageorgiou, V.; Kitchel, B.; Kaplan, D. L. *Biomacromolecules* **2006**, *7*, 3139–45.
- (48) Ene, R.; Papadopoulos, P.; Kremer, F. *Vib. Spectrosc.* **2011**, *57*, 207–12.
- (49) Yu, P. Q. *Br. J. Nutr.* **2005**, *94*, 655–65.
- (50) Bramanti, E.; Catalano, D.; Forte, C.; Giovanneschi, M.; Masetti, M.; Veracini, C. A. *Spectrochim. Acta, Part A* **2005**, *62*, 105–111.
- (51) Sunabori, T.; Tokunaga, A.; Nagai, T.; Sawamoto, K.; Okabe, M.; Miyawaki, A.; Matsuzaki, Y.; Miyata, T.; Okano, H. *J. Cell Sci.* **2008**, *121*, 1204–12.
- (52) Fanarraga, M. L.; Avila, J.; Zabala, J. C. *Eur. J. Neurosci.* **1999**, *11*, 517–27.
- (53) Mullen, R. J.; Buck, C. R.; Smith, A. M. *Development* **1992**, *116*, 201–11.
- (54) Shoulders, M. D.; Raines, R. T. *Annu. Rev. Biochem.* **2009**, *78*, 929–58.
- (55) Emsley, J.; Knight, C. G.; Farndale, R. W.; Barnes, M. J.; Liddington, R. C. *Cell* **2000**, *101*, 47–56.
- (56) Matthews, J. A.; Wnek, G. E.; Simpson, D. G.; Bowlin, G. L. *Biomacromolecules* **2002**, *3*, 232–238.
- (57) Albertson, A. E.; Teule, F.; Weber, W.; Yarger, J. L.; Lewis, R. V. *J. Mech. Behav. Biomed. Mater.* **2014**, *29*, 225–34.
- (58) Elices, M.; Plaza, G. R.; Perez-Rigueiro, J.; Guinea, G. V. *J. Mech. Behav. Biomed. Mater.* **2011**, *4*, 658–69.
- (59) Leipzig, N. D.; Shoichet, M. S. *Biomaterials* **2009**, *30*, 6867–78.
- (60) Wang, Y.; Wang, G.; Luo, X.; Qiu, J.; Tang, C. *Burns* **2012**, *38*, 414–20.
- (61) Ahmed, M. R.; Venkateshwarlu, U.; Jayakumar, R. *Biomaterials* **2004**, *25*, 2585–94.
- (62) Yamauchi, M.; Sricholpech, M. *Essays Biochem.* **2012**, *52*, 113–33.
- (63) Silver, F. H. *Collagen Relat. Res.* **1982**, *2*, 219–29.
- (64) Cheung, D. T.; Perelman, N.; Ko, E. C.; Nimni, M. E. *Connect. Tissue Res.* **1985**, *13*, 109–15.
- (65) Marriott, R. H. *Biochem. J.* **1932**, *26*, 46–53.
- (66) Brannvall, K.; Bergman, K.; Wallenquist, U.; Svahn, S.; Bowden, T.; Hilborn, J.; Forsberg-Nilsson, K. *J. Neurosci. Res.* **2007**, *85*, 2138–46.
- (67) Ma, W.; Tavakoli, T.; Derby, E.; Serebryakova, Y.; Rao, M.; Mattson, M. *BMC Dev. Biol.* **2008**, *8*, 90.
- (68) Campos, L. S. *BioEssays* **2005**, *27*, 698–707.
- (69) Persad, S.; Dedhar, S. *Cancer Metastasis Rev.* **2003**, *22*, 375–84.
- (70) Lariviere, R. C.; Beaulieu, J. M.; Nguyen, M. D.; Julien, J. P. *Neurobiol. Dis.* **2003**, *13*, 158–66.
- (71) Matsuda, M.; Katoh-Semba, R.; Kitani, H.; Tomooka, Y. *Brain Res.* **1996**, *723*, 177–89.
- (72) Lee, J.; Abdeen, A. A.; Zhang, D.; Kilian, K. A. *Biomaterials* **2013**, *34*, 8140–8.
- (73) Frith, J. E.; Mills, R. J.; Cooper-White, J. J. *J. Cell Sci.* **2012**, *125*, 317–27.
- (74) Forte, G.; Carotenuto, F.; Pagliari, F.; Pagliari, S.; Cossa, P.; Fiaccavento, R.; Ahluwalia, A.; Vozzi, G.; Vinci, B.; Serafino, A.; Rinaldi, A.; Traversa, E.; Carosella, L.; Minieri, M.; Di Nardo, P. *Stem Cells* **2008**, *26*, 2093–103.
- (75) Jones, E. N. B.; Mallapragada, S. K. *J. Biomater. Sci., Polym. Ed.* **2007**, *18*, 999–1015.
- (76) Cullen, D. K.; Wolf, J. A.; Smith, D. H.; Pfister, B. J. *CRC Crit. Rev. Bioeng.* **2011**, *39*, 241–59.
- (77) Polikov, V. S.; Tresco, P. A.; Reichert, W. M. *J. Neurosci. Methods* **2005**, *148*, 1–18.
- (78) Musallam, S.; Bak, M. J.; Troyk, P. R.; Andersen, R. A. *J. Neurosci. Methods* **2007**, *160*, 122–7.